2020

Oscillating column and triboelectric nanogenerator for ocean wave energy

Reilly, S.; Kwon, Y.W.

Springer

Reilly, S., and Y. W. Kwon. "Oscillating column and triboelectric nanogenerator for ocean wave energy." Multiscale and Multidisciplinary Modeling, Experiments and Design 3.1 (2020): 23-32.
http://hdl.handle.net/10945/65680

Multiscale and Multidisciplinary Modeling, Experiments and Design (2020) 3:23–32
https://doi.org/10.1007/s41939-019-00057-y

ORIGINAL PAPER

Oscillating column and triboelectric nanogenerator for ocean wave energy

S. Reilly[1] · **Y. W. Kwon**[1]

Received: 18 June 2019 / Accepted: 22 July 2019 / Published online: 6 August 2019

Abstract
This paper investigated energy harvesting from ocean waves using an oscillating column (OC) and a triboelectric nanogenerator (TENG). First, preliminary tests were conducted for a TENG fabricated using copper alloy or pure copper and polytetrafluoroethylene (PTFE) tape. Then, an OC was designed and built with the pure copper TENG, which was tested previously. The final design was tested in a tow tank with a wave maker to demonstrate the OC–TENG system under simulated ocean waves. The study examined different parameters that influenced the power generation, i.e., the voltage of alternative currents, in order to determine what parameters are critical to higher power generation.

Keywords Energy harvest · Oscillation column · Triboelectric nanogenerator · Ocean wave

1 Introduction

The world uses additional amounts of technology and devices that require electricity every single day. This leads to the increasing desire for further ways to generate electricity. For a long time, humans have depended on the use of fossil fuels for electrical power. As a result, one of the greatest global threats has emerged: global warming.

In response to the impacts of global warming, there have been advances in green energy (wind and solar energy) adding to the power grids of many nations. The use of these innovative technologies has helped decrease the burning of fossil fuels. Yet, there is still a lot of room for improvement to find additional alternate energy sources that have lower environmental impact than fossil fuels.

Nearly, 71% of the globe is covered in water. Of this 71%, about 96.5% is found in the oceans (USGS 2018). This equates to 68.5% of the world being water found in the ocean. In addition, about 44% of the population of the world lives within 150 km of the coast (Tollefson 2014). The basis of energy from oceans is a wave. Waves are naturally found in the oceans due to wind and the gravitational pull of the sun and the moon (National Ocean Service 2018).

✉ Y. W. Kwon
ywkwon@nps.edu

[1] Department of Mechanical and Aerospace Engineering, Naval Postgraduate School, Monterey, CA 93943, USA

Blue energy is the name given to the energy found in the waves of the ocean. A multitude of different advances have been made in the systems to extract blue energy. The use of blue energy offers many benefits such as minimal environmental impact, the ability of waves to travel long distances without losing much energy, and the accessibility of being able to use wave energy devices about 90% of the time (compared to availabilities of about 20–30% of the time with solar and wind energy devices). The technology to harvest this energy has over 1000 patents in Japan, North America and Europe. These technologies are usually differentiated by their location and type (Drew et al. 2009).

The three main locations for blue energy devices are shoreline, nearshore and offshore. Shoreline is considered to be in the shallow water near the shore. The shoreline devices have the advantages of being close to land and easier to maintain. In addition, they have a lower chance of being damaged in extreme weather conditions as they could be removed if harsh seas are predicted. One disadvantage is that as a result of being in shallow water, the waves tend to have less power near the shore. Nearshore devices are located a bit farther out into the water, but still have the ability to be attached to the seabed. Nearshore devices tend to have the same disadvantage as the shoreline devices of not being able to take advantage of more powerful waves due to their shallow water location. Offshore devices are generally found in deep water. Deep water devices tend to be more expensive, difficult to construct, and maintain due to being further from

the shore and encountering more extreme conditions (greater wave heights and energies). Yet, these more powerful waves can lead to greater power generation (Drew et al. 2009).

The three major types of wave energy devices are attenuators, point absorbers, and terminators. Attenuators are positioned parallel to the direction the wave is traveling. Point absorbers are small compared to the wavelength they are harvesting the energy from and tend to gather energy from the rising and falling motion of waves. Terminators are positioned perpendicular to the direction that the wave is traveling (Drew et al. 2009).

Of the over 1000 different patents, they can all be divided into one of these three locations (shoreline, nearshore, off shore) and one of these three types (attenuators, point absorbers, terminators) (Drew et al. 2009). Another way to further classify a wave energy device is by their mode of operation. There is a plethora of modes of operations for wave energy devices, but some of the major ones are submerged pressure differential, oscillating wave surge converter, oscillating water column and overtopping device. A submerged pressure differential device is a type of point absorber that utilizes the pressure differential between the troughs and crests of a wave. A wave surge oscillator is a type of terminator that utilizes the horizontal velocity of waves. An oscillating water column could act as either a point absorber or a terminator if it attached to the shoreline. An oscillating water column utilizes a chamber filled with air and the water level that is open to the motion of the wave. As the wave goes through the chamber, pressure is applied to the air through the motion of the wave and is usually pushed through a turbine. An overtopping device has the waves going over it and collects the energy of the wave through a turbine, which then releases the water back out (Drew et al. 2009).

The potential to use the power found in the waves of the ocean as a renewable energy is high. There is a wide variety of types and locations for devices with the ability to capture the energy found in ocean waves. Prior reviews of these technologies came to similar conclusions (Falcão 2008; Sun et al. 2018). Those conclusions are that the potential is very high, but it is expensive to make, deploy, test and maintain the devices, so progress in the research is slow to develop.

Triboelectricity is found in the electrostatic phenomenon and commonly found through friction. In the past, this friction has caused a design concern for devices with the presence of charges where they are not beneficial or could be dangerous. Now these charges are being seen as something that could be utilized to power devices. These charges could be a solution to the current need for more clean and renewable energy by utilizing what is already available in our daily life. The first triboelectric nanogenerator (TENG) was introduced in 2012 by the same group that successfully used the piezoelectric nanogenerator (Fan et al. 2012). The development of the TENG in 2012 was the beginning of research into harnessing triboelectricity with devices that produce usable electricity from mechanical energy while maintaining low cost and high durability.

The first TENG that was developed in 2012 used two thin polymer films pressed together, Kapton (polyimide) and polyester (PET). On the nanoscale, these two materials have different roughness, which allows for friction through a relative sliding between the two materials when the TENG is operated. The primary operation of this TENG was achieved through the bending of the stack of materials. On the outside of each of the polymers was a thin layer of aluminum alloy. This aluminum produced equal but opposite charges than the polymer it was attached to and allowed the TENG to be connected to an external circuit to examine the electrical outputs (Fan et al. 2012).

Since the introduction of the first TENG in 2012, a great deal of different types of TENGS was developed. These TENGS can be classified into four different working modes. These four modes are vertical contact-separation mode, single-electrode mode, freestanding triboelectric-layer mode, and contact-sliding mode (Wu et al. 2019).

The concentration of this research is using the contact-sliding mode of the TENG. The basic mechanism of the contact-sliding mode TENG was well explained in Ref. (Wang 2014, 2017). The current flow depends on how the two materials are matched with each other. This sliding TENG has been modeled (Niu et al. 2013) and proven to work with linear-grating (Zhu et al. 2013) and checker-like interdigital electrodes (Guo et al. 2015).

In the past 7 years since the TENG was first introduced, it has continued to have further developments and uses. The application of the TENG is broken down into two major categories: harvesting from the environment or self-powered devices/sensors (Ma et al. 2018). One of the large research areas with the TENG is using the mechanical energy found in water. There are two types of mechanical energy typically found in water, one from the motion of the water flowing, and the other from the motion of the waves (Xi et al. 2017). There is a large amount of research that has been completed with the TENG for both capturing the energy from the motion of flowing water (Cheng et al. 2014; Liang et al. 2015a, b, 2016; Lin et al. 2013; Zhang et al. 2017; Wang et al. 2016; Lee et al. 2016) and the motion of water waves (Xiao et al. 2018; Xu et al. 2016, 2018; Wen et al. 2016; Lee et al. 2018; Su et al. 2014; Chen et al. 2015; Zhu et al. 2014; Saadatnia et al. 2017). One TENG has been developed with the ability to harness the water energy from both the motion of the water and the motion of the waves in addition to the wind energy (Xi et al. 2017). The focus of this research is on harvesting mechanical energy from the environment, specifically harvesting blue energy from the motion of waves using a lateral-sliding mode TENG.

2 Design, fabrication and experiment of TENG

This section describes the design, fabrication and experimentation of a TENG device. The main design concept was similar to that in Ref. (Seol et al. 2017), which was the interdigitated design of the electrode pieces. One major consideration while developing a TENG is the selection of the materials to be used. A successful TENG uses two materials that are far away from each other on the triboelectric series so the electrons could be easily transferred between the two materials (Diaz and Felix-Navarro 2004). The transfer of these electrons between the two materials is what causes the triboelectricity. The two main materials chosen to be used for TENG were copper and polytetrafluoroethylene (PTFE) tape. The choice of these two materials was inspired by a TENG made of Teflon tape and conductive copper foil tape (Xia et al. 2018). These two materials are cost effective and on opposite sides of the triboelectric series.

The block of the TENG where the electrodes were placed into was modeled and designed as shown in Fig. 1. The spaces for the fingers of the electrodes were made to a depth of 0.5 mm and at the end, the depth was increased slightly to allow for soldering at the end of the electrode. This piece was 3D printed using an Ultimaker 3 Extended. Then, a piece of copper alloy as well as pure copper was machined to fit inside the block. Wires were then soldered onto the ends of the electrodes to allow for AC voltage readings from the TENG in operation. These copper electrodes are shown in Fig. 2.

The track for the TENG to slide on was also modeled and designed as shown in Fig. 3. This track was also 3D printed. The adhesive PTFE tape was then added to the track as shown in Fig. 4. This track was set to be an inner width of 67 mm to prevent any friction on the sides of the TENG and strictly allow friction at the interface of the PTFE tape and the copper

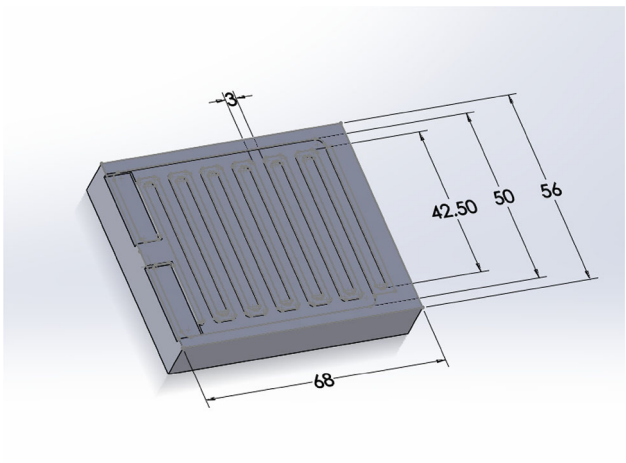

Fig. 1 Design for the electrode holder of the TENG (units in millimeter)

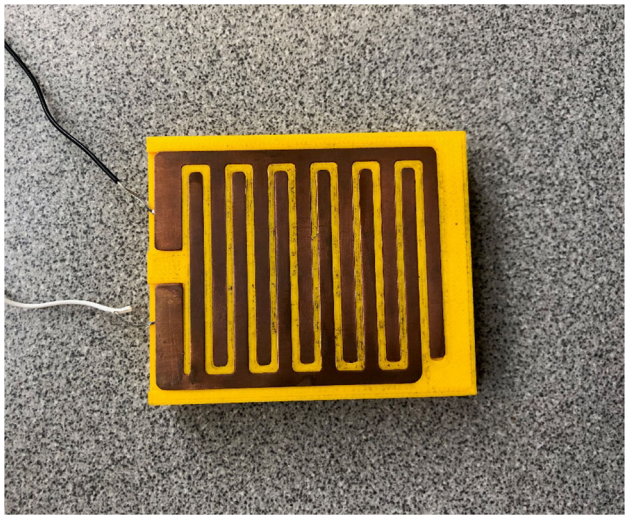

Fig. 2 Electrodes in the holder

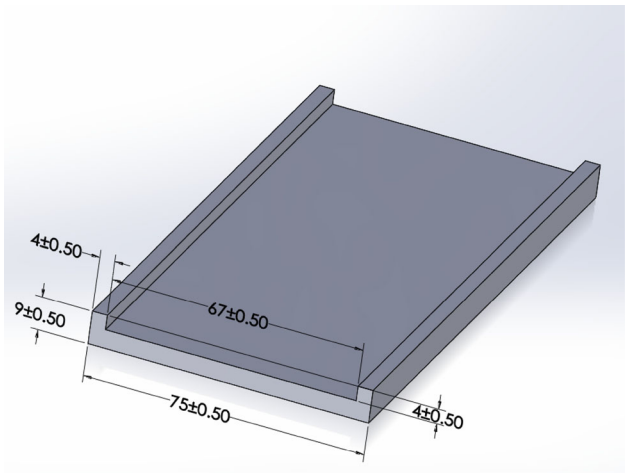

Fig. 3 Model of track of TENG (units in millimeter)

electrodes. The length of the track was 155 mm to allow a full sliding motion of the TENG electrode length.

A linear reciprocating motor was wired and set up for the testing of the TENG. It allowed for the speed and the contact force of the TENG to be regulated. A small connector piece was made to connect the TENG to the reciprocating motor as shown in Fig. 5. The figure shows a little disk that sat on top of the TENG that was created to test the TENG at different contact forces. All those pieces were 3D printed.

This setup was then tested at two different speeds with the linear motor, one at 50% speed and one at full speed. Each of these speeds was also tested with three different weight conditions on the weight plate. The first condition was without any additional weight. The next condition that was tested was with one block of mass (32 g) or three blocks of mass (96 g) on the weight plate.

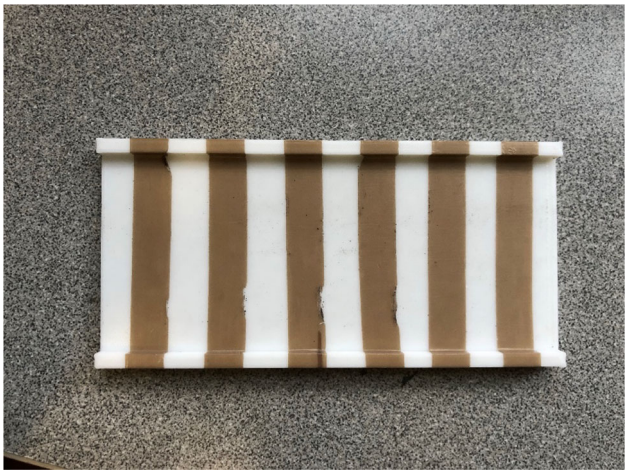

Fig. 4 3D Printed final track with adhesive PTFE tape

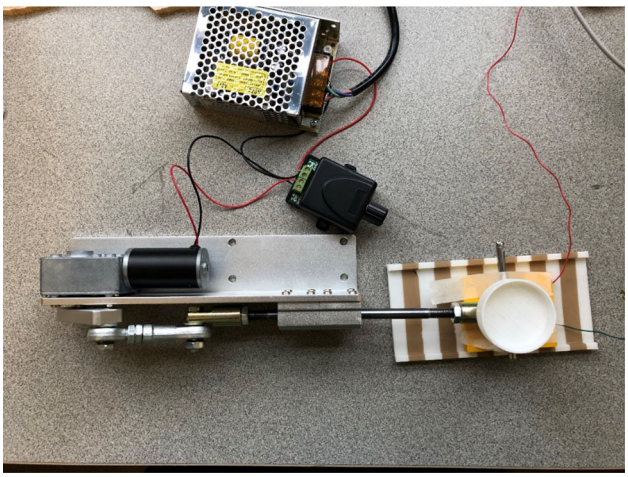

Fig. 5 Top view of the TENG setup attached to reciprocating linear motor

The experimentation was run with copper alloy and pure copper electrodes, respectively. Each electrode case was tested with three different weight conditions and two different speeds. These six different runs were each performed three times to make sure that the data were repeatable. The AC voltage outputs were measured with a Keysight DSO1052B digital oscilloscope.

3 Experimental results of TENG

The first set of results was obtained using the copper alloy electrodes. The first test was conducted with the reciprocating motor run at half speed (frequency of 2.083 Hz for the pulses). This run had no weight added in the weight holder. The result from the first run is shown in Fig. 6. The AC voltage outputs for this TENG were in a pulsing pattern. For this TENG test, there is a closer gap between the two pulses for a forward

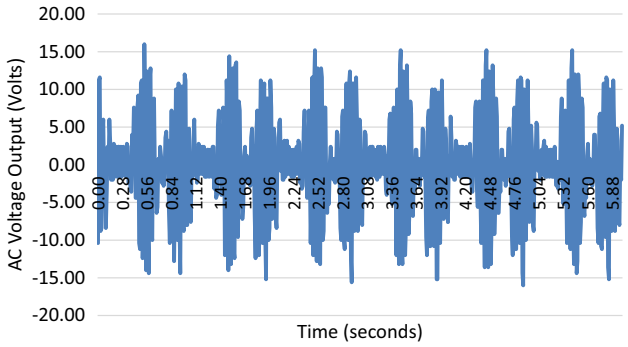

Fig. 6 AC voltage output from copper alloy electrodes with no additional weight and 2.083 Hz frequency

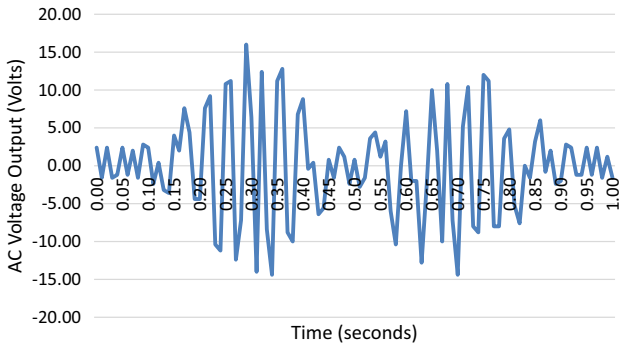

Fig. 7 A zoom-in view of AC voltage output from copper alloy electrodes with no additional weight and 2.083 Hz frequency

and backward movement of the TENG, which was one cycle of the linear motor. Then, as the motor went to go forward again, there was a little bit of a longer pause in the data. A zoom-in of this pulse pair is shown in Fig. 7. From this run, one can see that the range of the peak-to-peak is 32 v.

Figure 7 shows how the TENG has the pairs of pulses that are close together which correspond to the complete cycle of the linear motor. One can observe that the first pulse (forward motion) has the most positive maximum and the second pulse (backward motion) has the most negative minimum. This condition was run three separate times to verify that the data were repeatable. The average peak-to-peak for those three runs was 31.5 v.

Then, the weight was added to the system to increase the contact force and this was repeated with the full speed (4.167 Hz) of the reciprocating motor. The general characteristics of the AC voltage output are the same as shown in Figs. 6 and 7 except for the actual values.

After completing all set of planned tests, the copper alloy TENG was then moved by a human hand at a fast speed to find the maximum output the original TENG could possibly create. Although it is not possible to determine the contact force (weight) applied by the hand, it is possible to see the frequency associated with the maximum peak-to-peak AC voltage output.

Table 1 Summary of copper alloy TENG test with linear reciprocating motor

Frequency (Hz)	Added weight (g)	Average (for 3 runs) Maximum peak-to-peak AC output voltage (V)
2.08	0.00	31.47
2.08	32.00	30.67
2.08	96.00	27.33
4.17	0.00	62.00
4.17	32.00	61.83
4.17	96.00	67.60
10.35	N/A	446.67

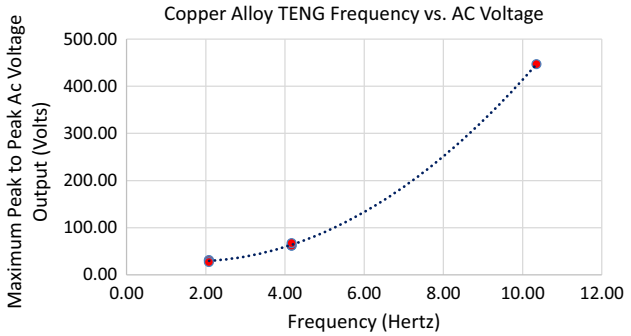

Fig. 8 TENG frequency and AC voltage for copper alloy TENG with wide PTFE tape

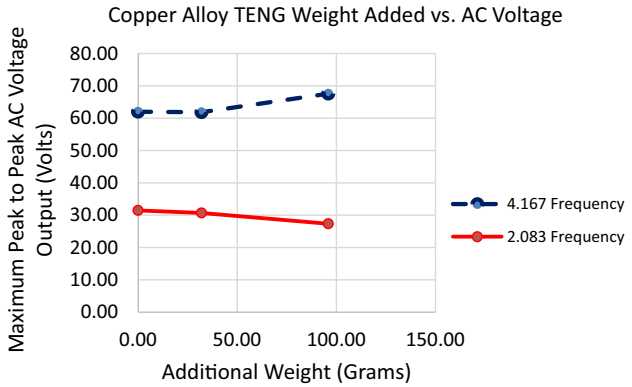

Fig. 9 Additional weight and AC voltage for copper alloy TENG

Table 2 Summary of copper TENG tests with linear reciprocating motor

Frequency (Hz)	Added weight (g)	Average (for 3 runs) Maximum peak-to-peak AC output voltage (V)
2.08	0.00	64.33
2.08	32.00	71.60
2.08	96.00	74.13
4.17	0.00	151.33
4.17	32.00	166.00
4.17	96.00	169.67
10.40	N/A	641.33

For the copper alloy TENG, the first run showed that there could be a maximum peak-to-peak AC output voltage of 448 v. This test was completed at a frequency of 10.4 hz. For the three tests run, the average maximum peak-to-peak AC output voltage was 447 v. Those three tests had an average frequency of 10.4 hz.

The results showed that there were some trends between the frequency the TENG was operated at and the maximum peak-to-peak AC output voltage. The summary of results of the maximum peak-to-peak AC output voltage, its corresponding frequency and added weight is shown in Table 1. The trend with frequency with the copper alloy TENG is that as the frequency increased, the maximum peak-to-peak AC voltage output also increased. This is increasing nonlinearly based on the data points collected, as shown in Fig. 8.

There was no trend found for the weight added to the copper alloy TENG and the AC output voltage. The results from the two different frequencies are shown in Fig. 9. For the higher frequency of 4.167 Hz, the maximum peak-to-peak AC output voltage went up with the additional weights added. However, for the lower frequency of 2.083 Hz, the maximum peak-to-peak output voltage decreased with the additional weights added. Therefore, for the copper alloy TENG, it was concluded that a higher frequency led to a higher maximum peak-to-peak AC output voltage, but the additional weights did not have a major impact on the voltage.

The next set of tests was undertaken using the pure copper electrodes. The previous experiments were repeated for the pure cooper TENG. As expected, the pure cooper TENG produced greater AC voltages than the copper alloy TENG under the same test condition. Table 2 gives the summary of test results for the pure copper TENG. Just as was observed with the frequency increase with the copper alloy TENG, the pure copper TENG also had an increase in the maximum peak-to-peak AC voltage output. This trend is shown in Fig. 10.

The trend between frequency and maximum peak-to-peak AC voltage output for the pure copper TENG has a bit more linear, but still nonlinear, trend than what was seen with the copper alloy TENG. It was clear that the increase in frequency directly correlated to an increase in AC voltage.

Upon further analysis of the pure copper TENG tests with the two speeds and three weight conditions, peak-to-peak AC voltage output also increased with the additional weight added. Although the impact of the additional weight was not as significant as the frequency, there was a consistent trend that as the weight was added, the peak-to-peak AC voltage output increased. The direct influence of the additional weight on the maximum peak-to-peak AC output voltage

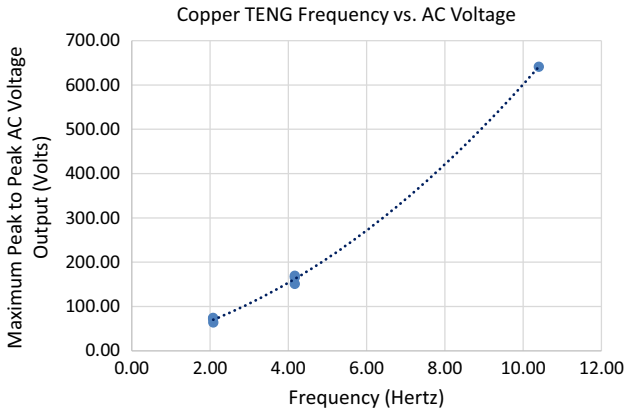

Fig. 10 TENG frequency and AC voltage for copper TENG with wide PTFE tape

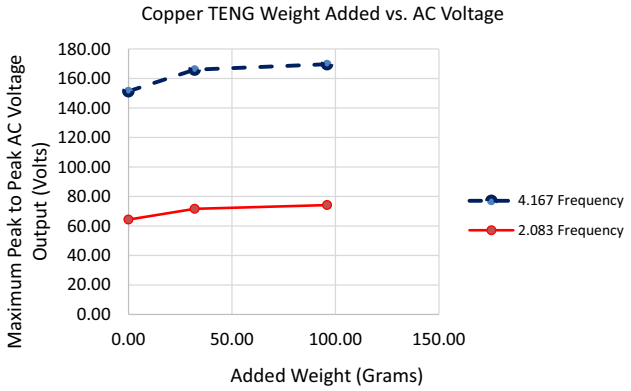

Fig. 11 Additional weight and AC voltage of improved TENG

was also analyzed for the pure copper TENG. The results are shown in Fig. 11.

As shown in Fig. 11, there was a trend between the added weight and frequency with the pure copper TENG. For both the fast frequency (4.167 Hz) and the slow frequency (2.083 Hz), the maximum peak-to-peak AC output voltage increased with the addition of more weight. Although this trend between added weight and AC voltage was found for the pure copper TENG, the dominating factor for higher AC voltage for both copper alloy and pure copper TENGS is to have the TENG operating at higher frequencies.

The additional testing condition to the pure copper TENG was a change in the thickness of the PTFE in the track. For this new track, the pure copper TENG was tested with the linear reciprocating motor at full speed. In addition, there were two weight conditions: one with no added weight and one with three blocks (96 g) of added weight. This created two new conditions to be completed with the pure copper TENG. Each of these conditions was run three times to ensure the reliability of the data.

The first run with the thinner PTFE tape track was with no added weight and the motor at full speed. The average maximum peak-to-peak AC output voltage for the three runs with this condition was 121 V. This is about 30 V less than the same speed and weight conditions for the copper TENG and the wider PTFE tape. The second condition with the thinner PTFE tape was completed with the linear reciprocating motor at full speed and the weight of three blocks of mass (96 g) in the weight holder. The average maximum peak-to-peak AC output voltage for the three runs at this condition was 146.7 V. This is about 20 V less than the pure copper TENG under the same conditions with the wider pieces of PTFE tape on the track. It was concluded that having the thinner PTFE tape was not beneficial to get the maximum AC voltage output of the copper TENG.

Following the testing of the copper TENG with the linear reciprocating motor, it was desired to be able to predict the maximum peak-to-peak AC output voltage for different frequencies. This would allow a user to achieve the maximum peak-to-peak AC output voltage by applying a certain frequency to the TENG. The bases of this model were made from the experimental results with the pure copper TENG and no additional weight condition. The goal of this simplified model was to be able to predict the upper half of the AC voltage signals produced. Equation (1) was used to calculate the models prediction for AC voltage output for each time step.

$$V(t) = V_{\text{peak}} \sin(2\pi\omega t) \tag{1}$$

where V_{peak} was determined based on the experimental data from the TENG testing with the linear reciprocating motor. From the test data, $V_{\text{peak}} = 1.955\omega^2 + 9.925\omega$. Here, ω is in Hz. For the slow frequency of 2.083 Hz, Eq. (1) resulted in V_{peak} of 29.2 V and a peak voltage of 75.3 V for the fast frequency of 4.167 Hz. These values represented the measured voltages closely.

4 Experiment and results of oscillating column and TENG

The next step in this research was to combine the TENG with a device that could extract the energy found in water waves. An oscillation column (OC) was the device used for this purpose. The OC is a type of point absorber because the whole column oscillates with the water falling and rising with the wave. The OC was restricted to only be able to operate in the heave (vertical) direction, thus giving the TENG linear-sliding motion.

An acrylic column with a diameter of 25.4 cm and a height of 24.5 cm was the main component of the OC. The thickness of the column was 0.397 cm. The bottom of the column was closed off, but the top was open. A cap for the column with a height of 12.7 cm and a 2.54 cm hole in the center was

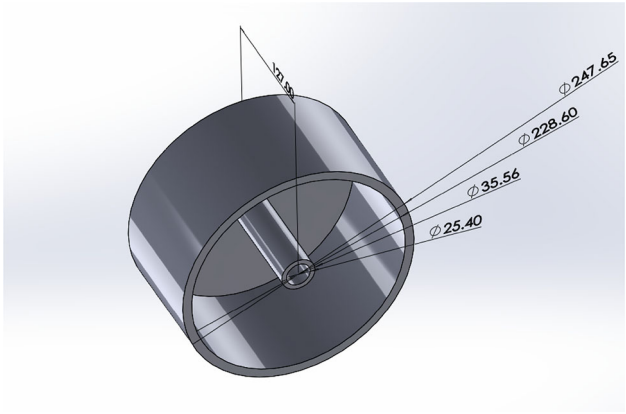

Fig. 12 Bottom view of the cap model for OWC (units in millimeters)

designed to fit inside the column. This cap was designed to make sure the column operated strictly in the heave direction and did not have a moment from the incident waves. The cap was 3D printed using the Fortus 400mc and the drawing of the model is shown in Fig. 12.

A block with one flat side and one curved side was then built to attach the TENG to the OC cap, which was then glued into the column to a depth that would allow the block and TENG to be attached to the side of it. A photo of the final OWC with the TENG attached to it is shown in Fig. 13.

The overall height of the structure was 33.02 cm after the cap was attached. Following the construction of the TENG with the OC, a hole was drilled into a piece of wood to fit across the width of the wave tank. A polyvinyl chloride (PVC) pipe was selected to have a tight fit through the hole in the wood, but have a looser fit through the hole in the cap of the OC. This kept the PVC pipe fixed but allowed the OC to heave along the pipe. In addition, a piece of wood was attached perpendicular to the piece of wood that spanned the width of the tank. This perpendicular piece of wood then had the TENG track attached to it. It was critical that the attachment of the perpendicular piece of wood and TENG track matched up with the TENG block so the triboelectricity could be generated. The final setup of the OC with the TENG attached and matching up with the TENG track in the wave tank is shown in Fig. 14.

The OC with the TENG attached was tested in the wave tank. It was tested with seven different frequencies of incident waves: 1.716 Hz, 1.475 Hz, 1.315 Hz, 1.200 Hz, 1.002 Hz, 0.903 Hz and 0.816 Hz. All these frequencies of waves were set to a wave amplitude of 2.54 cm, giving the waves a height of 5.08 cm. This wave height was selected to make sure the sliding motion of the TENG stayed within the length of the track. Each of these frequencies was run for two tests to verify the data. The AC voltage outputs were measured with a Keysight DSO1052B digital oscilloscope.

The highest frequency of wave used was 1.716 Hz. This was run for two tests and created a TENG frequency of about 3.43 Hz because for each wave the TENG had both an up and a down motion. The AC output voltage from these tests is shown in Fig. 15. Similar to the results seen when the TENG was tested with the linear reciprocating motor, the same pulsing of AC output voltage occurred. Yet, with this wave testing, the AC voltage outputs were much less than with the initial experimentation with the motor. The maximum peak-to-peak AC output voltage of run 1 was 14 V and of run 2 was 14.4 V.

The next frequency of wave used was 1.475 Hz. This created a TENG frequency of about 2.9 Hz. This was run for

Fig. 13 OWC with TENG and cap attached

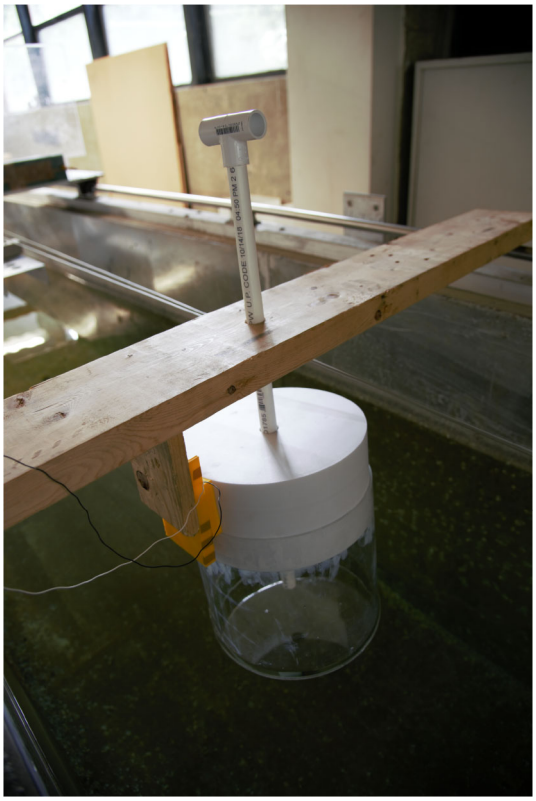

Fig. 14 Full setup of OWC with TENG attached in wave tank

two tests, and the wave frequency of 1.475 Hz produced a maximum peak-to-peak AC output voltage of 18.4 V for run 1 and 18 V for run 2. As shown in the test results, two runs for each wave frequency produced a very close AC voltage output. All the test results are summarized in Table 3.

Table 3 Summary of OWC-TENG testing

Wave frequency	TENG frequency	Average max peak-to-peak AC voltage
1.716	3.4	14.2
1.475	3.0	18.2
1.315	2.6	8.1
1.2	2.4	17.2
1.002	2.0	17.9
0.903	1.8	15.1
0.816	1.6	15

From the results of the testing of the OC and TENG in the wave tank, the TENG maximum peak-to-peak AC voltage outputs did not follow the same pattern with increasing frequency as it did with the linear reciprocating motor. There are some major operating differences between the linear motor TENG testing and the wave tank TENG testing. One of the major changes is that the TENG is operating in a horizontal motion during the linear motor testing, but during the wave tank testing it is operating in the vertical direction. In the vertical operating direction, it is difficult to maintain consistent contact forces between the TENG electrode and the TENG track. The TENG relies on the copper electrode and PTFE tape to be in contact to complete the circuit and generate voltage. Nonetheless, it is promising that there was AC voltage produced when the pure copper TENG was placed in the wave tank and tested; thus, triboelectricity was successfully created from waves.

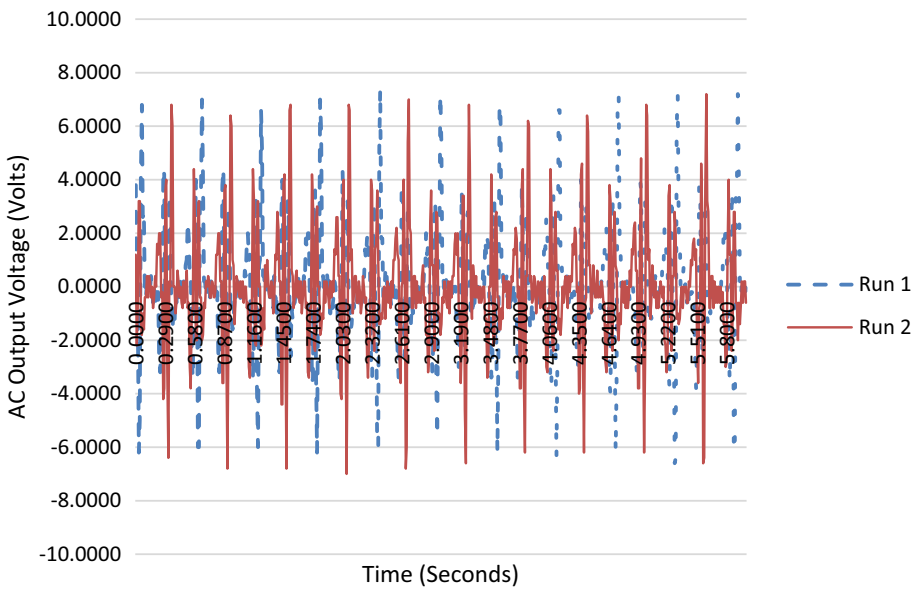

Fig. 15 AC output voltage of OWC-TENG with 1.716 Hz frequency of wave

5 Conclusions

The copper alloy TENG and the pure copper TENG were both tested with a linear reciprocating motor at two different frequencies and with three different weight conditions. It was found that for both the copper alloy TENG and the pure copper TENG the AC voltage output increased with an increase in the frequency at which the TENG operated. The average maximum peak-to-peak AC output voltage for the copper alloy TENG run for three tests by hand was found to be 447 V. The average maximum peak-to-peak AC output voltage for the pure copper TENG run for three tests by hand was found to be 641 V. There was no conclusive trend for the impact of the different weights on the copper alloy TENG. Yet, the pure copper TENG was found to have an increase in peak-to-peak AC output voltage with an increase in added weight. The TENG made of pure copper was then attached to an OC and ran against seven different wave frequencies in a wave tank. The pure copper TENG was successful at generating AC voltage when operating in the wave tank with the OC. There were not the same relationships between frequency and peak-to-peak AC voltage output with the pure copper TENG when it was operated in the wave tank as compared to when it was operated with the linear reciprocating motor. The maximum peak-to-peak AC output voltage for the pure copper TENG operating in the wave tank with the OC was 18.4 V and it was found at both the wave frequencies of 1.475 Hz and 1.002 Hz. This study was successful to demonstrate the coupled OC and TENG system for ocean wave application to harvest electricity.

Acknowledgements The authors appreciate Mr. Jarema Didoszak for his assistance throughout this research. We would like to thank LT Katherine Mann for her help in developing this Triboelectric Nanogenerator. Finally, we would like to thank John Mobley in Machine Lab, STG1 Corey Cauffiel in the Robodojo, and Mr. Daniel Sakoda for their help in fabricating parts for this project.

Compliance with ethical standards

Conflict of interest All authors state that there is no conflict of interest.

References

Chen J, Yang J, Li Z, Fan X, Zi Y, Jing Q, Guo H, Wen Z, Pradel K, Niu S, Wang ZL (2015) Networks of triboelectric nanogenerators for harvesting water wave energy: a potential approach toward blue energy. ACS Nano 9(3):3324–3331

Cheng G, Lin Z-H, Du Z-I, Wang ZL (2014) Simultaneously harvesting electrostatic and mechanical energies from flowing water by a hybridized triboelectric nanogenerator. ACS Nano 8(2):1932–1939

Diaz AF, Felix-Navarro RM (2004) A semi-quantitative tribo-electric series for polymeric materials: the influence of chemical structure and properties. J Electrostat 62:277–290

Drew B, Plummer AR, Sahinkaya MN (2009) A review of wave energy converter technology. Proceed Inst Mech Eng Part A J Power Energy 223(8):887–902

Falcão AF (2008) Wave energy utilization: a review of the technologies. Renew Sustain Energy Rev 14(3):899–918

Fan F, Tian Z, Wang ZL (2012) Flexible triboelectric generator. Nano Energy 1(2):328–334

Guo H, Leng Q, He X, Wang M, Chen J, Hu C, Xi Y (2015) A triboelectric generator based on checker-like interdigital electrodes with a sandwiched PET thin film for harvesting sliding energy in all directions. Adv Energy Mater 5(1):1400790

Lee S, Chung J, Kim DY, Jung J-Y, Lee SH, Lee S (2016) Cylindrical water triboelectric nanogenerator via controlling geometrical shape of anodized aluminum for enhanced electrostatic induction. ACS Appl Mater Interfaces 8(38):25014–25018

Lee K, Lee J-W, Kim K, Yoo D, Kim DS, Hwang W, Song I, Sim J-Y (2018) A spherical hybrid triboelectric nanogenerator for enhanced water wave energy harvesting. Micromachines 9(11):598

Liang QJ, Yan X, Liao X, Cao S, Zheng X, Si H, Lu S, Zhang Y (2015a) Multi-unit hydroelectric generator based on contact electrification and its service behavior. Nano Energy 16:329–338

Liang Q, Yan X, Gu Y, Zhang K, Liang M, Lu S, Zheng X, Zhang Y (2015b) Highly transparent triboelectric nanogenerator for harvesting water- related energy reinforced by antireflection coating. Sci Rep 5:9080

Liang Q, Yan X, Liao X, Zhang Y (2016) Integrated multi-unit transparent triboelectric nanogenerator harvesting rain power for driving electronics. Nano Energy 25:18–25

Lin Z-H, Cheng G, Lin L, Lee S, Wang ZL (2013) Water-solid surface contact electrification and its use for harvesting liquid-wave1 energy. Angew Chem 52:12545–12549

Ma M, Kang Z, Liao Q, Zhang Q, Gao F, Zhao X, Zhang Z, Zhang Y (2018) Development, applications, and future directions of triboelectric nanogenerators. Nano Res 11(6):2951–2969

National Ocean Service (2018) How important is the ocean to our economy? (Online). https://oceanservice.noaa.gov/facts/oceaneconomy.html. Accessed 8 Nov 2018

Niu S, Liu Y, Wang S, Lin L, Zhou Y, Hu Y, Wang ZL (2013) Theory of sliding-mode triboelectric nanogenerators. Adv Mater 25(43):6184–6193

Saadatnia Z, Asadi E, Askari H, Zu J, Esmailzadeh E (2017) Modeling and performance analysis of duck-shaped triboelectric and electromagnetic generators for water wave energy harvesting. Int J Energy Res 41(14):2392–2404

Seol M-L, Han J-W, Moon DI, Yoon KJ, Hwang CS, Meyyappan M (2017) All-printed triboelectric nanogenerator. Nano Energy 44:82–88

Su Y, Wen X, Zhu G, Yang J, Chen J, Bai P, Wu Z, Jiang Y, Wang ZL (2014) Hybrid triboelectric nanogenerator for harvesting water wave energy and as a self-powered distress signal emitter. Nano Energy 9:186–195

Sun C, Shang J, Luo Z, Lu Z, Wang R (2018) A review of wave energy extraction technology. IOP Conf Ser Mater Sci Eng 394:042038

Tollefson J (2014) Power from the oceans: blue energy. Nature 508(7496):302–304

USGS (2018) How much water is there on Earth? (Online). https://water.usgs.gov/edu/earthhowmuch.html. Accessed 8 Nov 2018

Wang ZL (2014) Triboelectric nanogenerators as new energy technology and self-powered sensors—principles, problems and perspectives. Faraday Discuss 176:447–458

Wang ZL (2017) On Maxwell's displacement current for energy and sensors: the origin of nanogenerators. Mater Today 00(00):1–9

Wang X, Wen Z, Guo H, Wu C, He X, Lin L, Cao X, Wang ZL (2016) Fully packaged blue energy harvester by hybridizing a rolling triboelectric nanogenerator and an electromagnetic generator. ACS Nano 10(12):11369–11376

Wen Z, Guo H, Zi Y, Yeh M-H, Wang X, Deng J, Wang J, Li S, Hu C, Zhu L, Wang ZL (2016) Harvesting broad frequency band blue energy by a triboelectric-electromagnetic hybrid nanogenerator. ACS Nano 10(7):6526–6534

Wu C, Wang AC, Ding W, Guo H, Wang ZL (2019) Triboelectric nanogenerator: a foundation of the energy for the new era. Adv Energy Mater 9(1):1802906

Xi Y, Guo H, Zi Y, Li X, Wang J, Deng J, Li S, Hu C, Cao X, Wang ZL (2017) Multifunctional TENG for blue energy scavenging and self-powered wind speed sensor. Adv Energy Mater 7(12):1602397

Xia K, Zhu Z, Zhang H, Du C, Wang R, Xu Z (2018) Cost-effective triboelectric nanogenerator based on teflon tape and conductive copper foil tape. Microelectron Eng 199:114–117

Xiao TX, Jiang T, Zhu JX, Liang X, Xu L, Shao JJ, Zhang CL, Wang J, Wang ZL (2018) Silicone-based triboelectric nanogenerator for water wave energy harvesting. ACS Appl Mater Interfaces 10(4):3616–3623

Xu L, Pang Y, Zhang C, Jiang T, Chen X, Luo J, Tang W, Cao X, Wang ZL (2016) Integrated triboelectric nanogenerator array based on air-driven membrane structures for water wave energy harvesting. Nano Energy 31:351–358

Xu L, Jiang T, Lin P, Shao J, He C, Zhong W, Chen XY, Wang ZL (2018) Coupled triboelectric nanogenerator networks for efficient water wave energy harvesting. ACS Nano 12(2):1849–1858

Zhang Q, Liang QL, Liao Q, Yi F, Zheng X, Ma M, Gao F, Zhang Y (2017) Service behavior of multifunctional triboelectric nanogenerators. Adv Mater 29:1606703

Zhu G, Chen J, Liu Y, Bai P, Zhou YS, Jing Q, Pan C, Wang ZL (2013) Linear-grating triboelectric generator based on sliding electrification. Nano Lett 13(5):2282–2289

Zhu G, Su Y, Bai P, Chen J, Jing Q, Yang W, Wang ZL (2014) Harvesting water wave energy by asymmetric screening of electrostatic charges on a nanostructured hydrophobic thin-film surface. ACS Nano 8(6):6031–6037